iScience

CellPress

Article

A Cancer-Associated Missense Mutation in PP2A-Aα Increases Centrosome Clustering during Mitosis

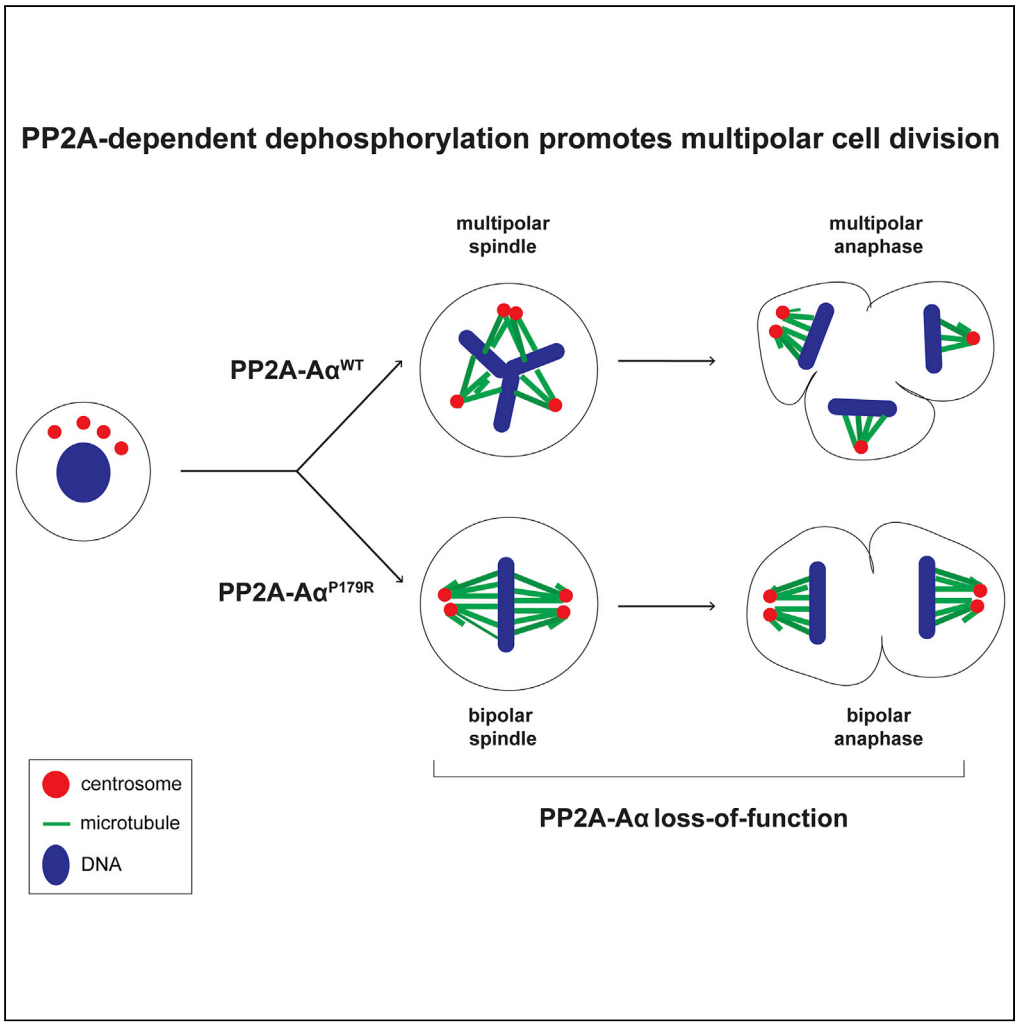

Noelle V. Antao, Marina Marcet-Ortega, Paolo Cifani, Alex Kentsis, Emily A. Foley

emilyafoley@gmail.com

HIGHLIGHTS

A heterozygous P179R mutation in PP2A-Aα decreases PP2A phosphatase assembly

Intracellular targeting of $PP2A^{B56\alpha}$ in mitosis is reduced in PP2A-$A\alpha^{P179R/+}$ cells

PP2A-$A\alpha^{P179R/+}$ cells are more proficient at centrosome clustering

Increased centrosome clustering is likely due to PP2A-Aα loss of function

Antao et al., iScience *19*, 74–82
September 27, 2019
https://doi.org/10.1016/j.isci.2019.07.018

iScience

CellPress

Article

A Cancer-Associated Missense Mutation in PP2A-Aα Increases Centrosome Clustering during Mitosis

Noelle V. Antao,[1,2] Marina Marcet-Ortega,[2] Paolo Cifani,[3] Alex Kentsis,[3] and Emily A. Foley[2,4,*]

SUMMARY

Whole-genome doubling (WGD) is common early in tumorigenesis. WGD doubles ploidy and centrosome number. In the ensuing mitoses, excess centrosomes form a multipolar spindle, resulting in a lethal multipolar cell division. To survive, cells must cluster centrosomes to allow bipolar cell division. Cancer cells are often more proficient at centrosome clustering than untransformed cells, but the mechanism behind increased clustering ability is not well understood. Heterozygous missense mutations in *PPP2R1A*, which encodes the alpha isoform of the "scaffolding" subunit of PP2A (PP2A-Aα), positively correlate with WGD. We introduced a heterozygous hotspot mutation, P179R, into *PPP2R1A* in human RPE-1 cells. PP2A-Aα^{P179R} decreases PP2A assembly and intracellular targeting in mitosis. Strikingly, PP2A-Aα^{P179R} enhances centrosome clustering when centrosome number is increased either by cytokinesis failure or centrosome amplification, likely through PP2A-Aα loss of function. Thus cancer-associated mutations in PP2A-Aα may increase cellular fitness after WGD by enhancing centrosome clustering.

INTRODUCTION

Most human tumors are aneuploid. In about one-third of tumors, aneuploidy is preceded by a whole-genome doubling (WGD) (Zack et al., 2013), an event that correlates with poor prognosis for patients (Bielski et al., 2018). After WGD, the newly tetraploid genome promotes the evolution of aneuploid karyotypes (Dewhurst et al., 2014), with tumor cells losing chromosomes and acquiring chromosomal rearrangements (Carter et al., 2012; Zack et al., 2013). However, WGD can be detrimental to subsequent mitoses because centrosome number doubles (from two to four) concomitantly with genome doubling. During mitosis, each centrosome nucleates microtubules (Ring et al., 1982), to form a multipolar spindle, which if uncorrected, can result in a lethal multipolar cell division (Ganem et al., 2009). Alternatively, cells can cluster supernumerary centrosomes into two spindle poles, to allow the formation of a pseudo-bipolar spindle (Quintyne et al., 2005), which permits bipolar cell division and survival. Given that centrosome amplification is common in cancers (Chan, 2011) and lethal multipolar cell divisions are expected to decrease the fitness of a tumor cell population, cancer cells likely experience selective pressures to efficiently cluster supernumerary centrosomes.

Human cells have an intrinsic ability to cluster centrosomes. This depends on proteins that directly or indirectly contribute to force generation during mitosis. Within the spindle, centrosome clustering arises from motor proteins located near spindle poles and centrosomes, such as dynein and KIFC1/HSET, as well as proteins localized at the kinetochore or centromere that control microtubule binding and spindle assembly checkpoint signaling (Drosopoulos et al., 2014; Kwon et al., 2008; Leber et al., 2010; Quintyne et al., 2005). Outside of the spindle, at the cell cortex, motor proteins associated with the cortical actin network, such as Myo10 and dynein, position centrosomes by generating force on astral microtubules (Kwon et al., 2015; Quintyne et al., 2005). Compared with non-transformed cells, centrosome clustering is more efficient in cancer cells (Ganem et al., 2009). Although centrosome clustering efficiency can be increased by depletion of the microtubule-binding protein NUMA (Quintyne et al., 2005) or the adhesion protein E-cadherin (Rhys et al., 2018), it remains largely unclear how cancer cells evolve to cluster centrosomes more proficiently.

Genomic analyses have identified genetic alterations that positively correlate with WGD (Bielski et al., 2018; Zack et al., 2013). Several changes (*TP53* and *RB1* mutation, *CCNE1* amplification) enable cell proliferation after WGD by alleviating the G1 arrest triggered after cytokinesis failure (Andreassen et al., 2001). The molecular impact of other genetic changes that positively correlate with WGD, including alterations in protein

[1]Program in Biochemistry and Structural Biology, Cell and Developmental Biology, and Molecular Biology, Weill Cornell Medicine Graduate School of Medical Sciences, Cornell University, New York, NY 10065, USA

[2]Cell Biology Program, Memorial Sloan Kettering Cancer Center, New York, NY 10065, USA

[3]Molecular Pharmacology Program, Memorial Sloan Kettering Cancer Center, New York, NY 10065, USA

[4]Lead Contact

*Correspondence: emilyafoley@gmail.com

https://doi.org/10.1016/j.isci.2019.07.018

phosphatase 2A (PP2A), is unknown. PP2A is a major source of serine/threonine phosphatase activity in eukaryotic cells. In the PP2A heterotrimer, a catalytic subunit (PP2A-Cα/β) and a "scaffolding" subunit (PP2A-Aα/β) are targeted to substrates by four evolutionarily conserved families of regulatory subunits. PP2A inactivation has been previously linked to tumorigenesis with the discovery that the SV40 small t antigen blocks the binding of PP2A-Aα/β to regulatory subunits (Pallas et al., 1990), leading to cellular transformation (Chen et al., 2004). Potentially similar perturbations in PP2A have been found to positively correlate with WGD in tumors. These include homozygous deletion of *PPP2R2A*, which encodes the B55α regulatory subunit, and heterozygous missense mutations in *PPP2R1A*, which encodes the α isoform of the scaffolding subunit PP2A-A, that accounts for ~90% of total PP2A-A (Zhou et al., 2003). Hotspot mutations in PP2A-Aα are expected to prevent B55 and B56 regulatory subunit binding (Cho and Xu, 2007; Xu et al., 2006, 2008) and thus likely decrease the functionality of PP2A-Aα. Indeed, functional inactivation of PP2A by a recurrent P179R mutation in *PPP2R1A* has been recently implicated as a driver of tumorigenesis in high-grade endometrial carcinoma (Taylor et al., 2019). In other studies, over-expression of certain hotspot PP2A-Aα mutants in tissue culture cells has been observed to alter phospho-signaling (Haesen et al., 2016; Jeong et al., 2016). However, the impact of PP2A-Aα missense mutations with respect to WGD has not been examined.

Here we examine the impact of two prevalent hotspot mutations in *PPP2R1A*, P179R and R183W, on PP2A holoenzyme assembly and find that a reduction in protein-protein interactions predominates and is shared between the two mutants. We then focus on the P179R mutation in *PPP2R1A*, as this mutation is linked to tumorigenesis (Taylor et al., 2019). When introduced into one allele of endogenous *PPP2R1A*, the P179R mutation reduces PP2A holoenzyme assembly and intracellular targeting of $PP2A^{B56}$ in mitosis. Strikingly, we find that these changes are sufficient to increase centrosome clustering after WGD, possibly in part through factors at the cell cortex that position centrosomes. Moreover, overexpression of wild-type PP2A-Aα partially rescues centrosome clustering, suggesting that this phenotype arises from a decrease in PP2A activity in mitosis.

RESULTS

Characterization of Prevalent Cancer-Associated PP2A-Aα Missense Mutations

PPP2R1A is most frequently mutated in uterine cancers (Figure 1A), and to explore the cellular impact of the two most frequent *PPP2R1A* missense mutations (Figure 1B), we generated retinal pigment epithelial (RPE-1) hTERT cell lines expressing GFP-tagged PP2A-Aα wild-type (WT), P179R, or R183W. Each construct was expressed at 30%–40% of the level of endogenous PP2A-Aα/β (Figure 1C). Using quantitative mass spectrometry, we compared the composition of PP2A complexes isolated from stable isotope labeling by amino acids in cell culture (SILAC)-labeled cells by immunoprecipitation of WT or mutant GFP-PP2A-Aα. The P179R mutation significantly reduced PP2A-Aα binding to four B56 regulatory subunits (B56α/*PPP2R5A*, B56β/*PPP2R5B*, B56δ/*PPP2R5D*, and B56ε/*PPP2R5E*). Accordingly, the binding of proteins that associate with PP2A-Aα via B56 subunits including GEF-H1 (*ARHGEF2*), Liprinα1 (*PPFIA1*) (Hertz et al., 2016), and *MTCL1* (Hyodo et al., 2016) was similarly reduced (Figure 1D). The P179R mutation also significantly reduced binding to the B55δ/*PPP2R2D* regulatory subunit (Figure 1D). The binding of STRN regulatory subunits (*STRN*, *STRN3*, and *STRN4*), a B″ regulatory subunit (*PPP2R3A*), and PP2A-C (*PPP2CA*, *PPP2CB*) was unaffected (Figure 1D). The R183W mutant had an overall similar decrease in protein-protein interactions (Figure 1E). Notably, although several proteins were observed to have increased binding to a PP2A-Aα mutant, none were shared between the two mutants (Figure 1F). Thus the major impact of both P179R and R183W mutations is to reduce protein-protein interactions.

A Heterozygous P179R Mutation in PP2A-Aα Impacts PP2A Holoenzyme Assembly in Human Cells

To examine if a heterozygous PP2A-Aα missense mutation is sufficient to impact PP2A functionality, we introduced a P179R mutation into one allele of endogenous *PPP2R1A* in RPE-1 cells. The P179R mutation was selected because it is the most prevalent missense mutation in uterine tumors, which have the highest incidence of PP2A-Aα alterations (Cerami et al., 2012). We used adeno-associated virus-mediated gene targeting (Berdougo et al., 2009) to introduce a C to G mutation in exon five of *PPP2R1A* (Figure 2A) and isolated two independent heterozygous clones (Figure 2B). The mutation did not alter the levels of PP2A-Aα or PP2A-Aα/β (Figure 2C). Similarly, PP2A-Aα immunoprecipitates from WT and $PP2A\text{-}A\alpha^{P179R/+}$ cells had equivalent levels of PP2A-C (Figure S1A) and phosphatase activity (Figure S1B). By contrast, we observed near-2-fold reductions in PP2A-Aα association with B56γ, δ, and ε (Figures 2D, 2E, and S1C) and B55α

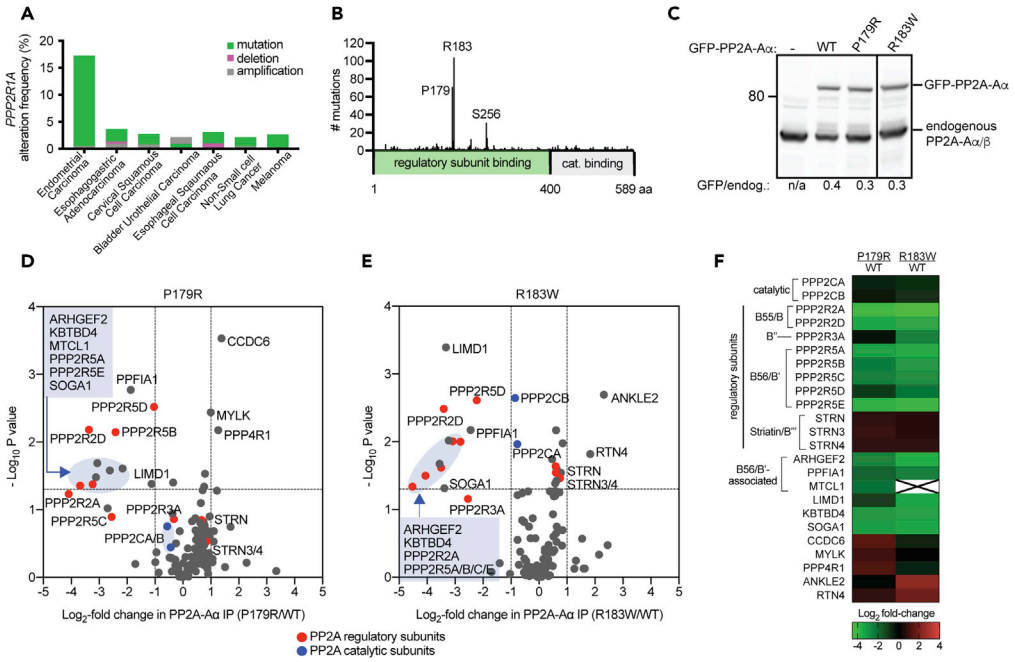

Figure 1. Quantitative Proteomic Characterization of Cancer-Associated PP2A-Aα Mutations

(A and B) Incidence of (A) *PPP2R1A* alterations and (B) missense mutations (Cerami et al., 2012; Gao et al., 2013).

(C) Western blot analysis of cells expressing GFP-PP2Aα-WT or indicated mutants. Solid line indicates intervening lanes have been removed.

(D and E) GFP immunoprecipitates from isotopically labeled RPE-1 cells expressing GFP-PP2A-Aα (WT, P179R, or R183W) were analyzed by mass spectrometry. Volcano plots with the mean $\log_2$ fold-change of proteins bound to mutant versus GFP-PP2Aα-WT against $-\log_{10}$ p value. 2-fold change (vertical dashed lines); $p < 0.05$ (horizontal dashed lines); red and blue circles indicate PP2A regulatory and catalytic subunits respectively.

(F) Heatmap of proteins with significant changes in association. Green to red gradient represents the mean $\log_2$ fold-change. X, protein not detected.

(Figures S1D and S1E). Consistent with a decrease in $PP2A^{B56}$ holoenzyme levels, intracellular targeting of both PP2A-Aα and B56α to the centromere or kinetochore was reduced in PP2A-$A\alpha^{P179R/+}$ cells (Figures 2F and 2G). Collectively, these results indicate that a heterozygous P179R mutation in PP2A-Aα is sufficient to alter the level of a subset of PP2A holoenzymes.

PP2A-$A\alpha^{P179R/+}$ Cells Suppress Multipolar Cell Division after Cytokinesis Failure

PPP2R1A mutations are enriched in tumors that experience WGD (Zack et al., 2013). Given that the levels of $PP2A^{B55}$ and $PP2A^{B56}$ holoenzymes were reduced in PP2A-$A\alpha^{P179R/+}$ cells, and that each of these holoenzyme families contribute to cell division (Craney et al., 2016; Espert et al., 2014; Foley et al., 2011; Kitajima et al., 2006; Lee et al., 2017; Nijenhuis et al., 2014; Schmitz et al., 2010), we considered the possibility that the P179R mutation in *PPP2R1A* might impact cells in mitosis following WGD. To test this, we induced one round of cytokinesis failure (Yang et al., 2008) by treating cells with cytochalasin D or B, inhibitors of actin polymerization (Cooper, 1987), or with blebbistatin, a myosin II inhibitor (Straight et al., 2003). Binucleate cells were imaged live during the ensuing mitosis (Figure 3A). To avoid a G1 cell-cycle arrest triggered by cytokinesis failure (Andreassen et al., 2001), we treated $Tp53^{+/+}$ cells with p38 inhibitor SB 203580 (Cuenda et al., 1995) or utilized $Tp53^{-/-}$ cells. Almost 30% of WT cells treated with cytochalasin D underwent multipolar cell divisions. Strikingly, PP2A-$A\alpha^{P179R/+}$ cells exhibited 4-fold reduction in the frequency of multipolar cell divisions compared with WT cells (7% in clone a and 8% in clone b) (Figures 3B and 3C). PP2A-$A\alpha^{P179R/+}$ cells also underwent fewer multipolar cell divisions when cytokinesis failure was induced with cytochalasin B or blebbistatin (Figure 3C). Similar results were observed in $Tp53^{-/-}$ PP2A-$A\alpha^{P179R/+}$ cells (Figure 3D). Notably, whereas the expression of PP2A-Aα -P179R in WT cells had no impact on the outcome of cell division, the expression of GFP-PP2A-Aα-WT in PP2A-$A\alpha^{P179R/+}$ cells partially rescued the cell division phenotype (Figures 3E and 3F), suggesting that the observed phenotype is likely due to haploinsufficiency.

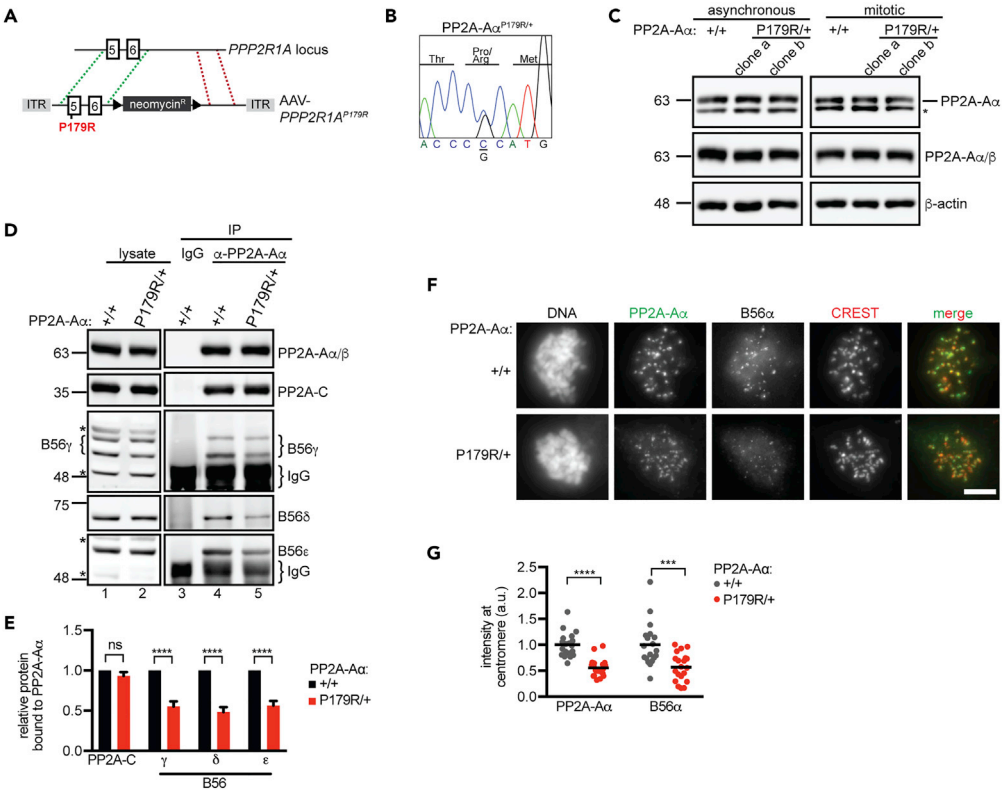

Figure 2. A Heterozygous P179R Mutation in PP2A-Aα Decreases PP2A^{B56} Assembly and Targeting

(A) Schematic of *PPP2R1A* gene-targeting strategy. Exons, rectangles; *loxP* sites, triangles; ITR, AAV-specific inverted tandem repeats; homologous sequences, green and red dashed lines.

(B) Sanger sequencing the modified region of *PPP2R1A* in a mutant clone.

(C) Western blot analysis of lysates from WT (+/+) and independently derived PP2A-Aα$^{P179R/+}$ (P179R/+) clones. * Shows non-specific band.

(D and E) (D) Western blot analysis of lysates (lanes 1–2) and immunoprecipitations (IPs) of control IgG (lane 3) or PP2A-Aα IgG (lane 4–5) in indicated cell lines. (E) Plotted is the normalized mean ± SEM of the experiment in (D) performed three times.

(F–G) WT (+/+) and PP2A-Aα$^{P179R/+}$ (P179R/+) cells in nocodazole were fixed and processed for immunofluorescence. (F) Maximum intensity projection. Scale bar, 5 μm. (G) Normalized centromere or kinetochore signal is plotted. Circle, cell; line, mean.

Result is representative of three experiments. ****$p < 0.00005$, ***$p < 0.0005$; ns, not significant ($p > 0.05$), calculated from Student's t test.

See also Figure S1.

Given that PP2A-Aα$^{P179R/+}$ cells have a modest delay in mitosis (22 min in clone a and 21 min in clone b versus 18 min in WT cells) (Figure S2A) and increased time spent in mitosis suppresses multipolar mitoses (Kwon et al., 2008), we next compared the mitotic duration of binucleate cells that underwent a bipolar cell division. Both WT and PP2A-Aα$^{P179R/+}$ cells completed mitosis with indistinguishable kinetics (Figure 3G). We also examined if the cell division phenotype was caused by centrosome inactivation as observed in *Drosophila* (Basto et al., 2008). However, microtubule nucleation was observed at all centrosomes in WT and PP2A-Aα$^{P179R/+}$ cells (Figure S2B). Moreover, in PP2A-Aα$^{P179R/+}$ cells, centrosomes were always associated with spindle poles (Figure S2C) and were more likely to be clustered (Figure S2D). Our data suggest that enhanced bipolar cell division after WGD in PP2A-Aα$^{P179R/+}$ cells is likely due to more efficient centrosome clustering and not due to centrosome inactivation or lengthening of mitosis.

PP2A-Aα$^{P179R/+}$ Cells Cluster Supernumerary Centrosomes More Efficiently

To test the hypothesis that PP2A-Aα$^{P179R/+}$ cells may cluster supernumerary centrosomes more efficiently than WT cells, centrosome amplification was induced by over-expression of Plk4 kinase

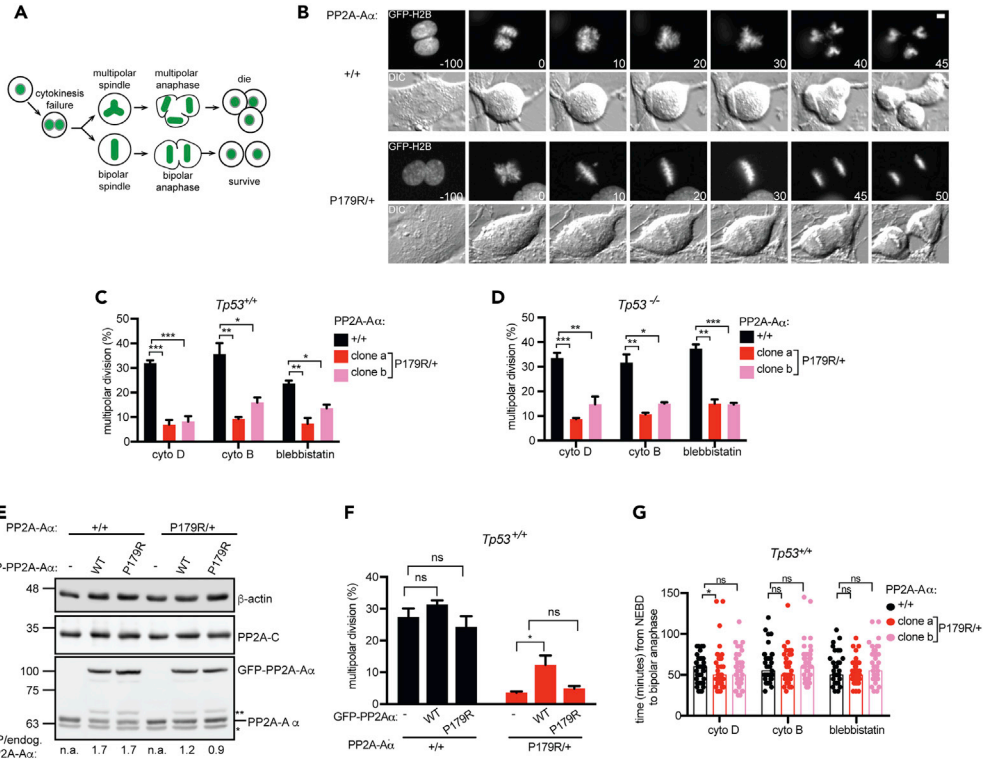

Figure 3. The P179R Mutation in PP2A-Aα Suppresses Multipolar Cell Division after Cytokinesis Failure

(A) Schematic of cytokinesis failure assay.

(B) GFP-H2B (top) and differential interference contrast (bottom) time-lapse images of WT (+/+) and PP2A-A$\alpha^{P179R/+}$ (P179R/+) cells after cytochalasin D treatment. Time (minutes) relative to nuclear envelope breakdown is indicated. Scale bar, 5 μm.

(C) Quantification of cell division outcome of *Tp53*$^{+/+}$ cells.

(D) Quantification of multipolar cell divisions in *Tp53*$^{-/-}$ cells treated as in (A).

(E and F) Cell lines of the indicated genotype expressing GFP-PP2A-Aα-WT or GFP-PP2A-Aα-P179R were (E) analyzed by western blot, where * shows non-specific band and ** shows GFP-PP2A-Aα truncation product, and (F) treated with cytochalasin D as in (A), imaged, and cell division outcome quantified.

(G) Mitotic duration of *Tp53*$^{+/+}$ cells in (C) undergoing bipolar cell divisions is plotted. Bars, median; circles, cells.

Result is representative of three experiments. (C, D, and F) Mean ± SEM from three experiments is plotted. ***$p < 0.0005$, **$p < 0.005$, *$p < 0.05$; ns, not significant ($p > 0.05$) Student's t test.

See also Figure S2.

(Kleylein-Sohn et al., 2007; Peel et al., 2007) (Figure 4A). This increases centrosome number without altering ploidy. We introduced a doxycycline-inducible Plk4 into *Tp53*$^{-/-}$ WT and PP2A-A$\alpha^{P179R/+}$ cells. After doxycycline induction, immunofluorescence analyses of C-Nap1, a marker of functional centrioles (Wang et al., 2011), indicated that 64% of WT cells and 68% of PP2A-A$\alpha^{P179R/+}$ cells had centrosome amplification (Figures S2E and S2F). Immunofluorescence analysis of anaphase cells with extra centrosomes revealed that PP2A-A$\alpha^{P179R/+}$ cells clustered centrosomes into a bipolar spindle more efficiently than WT cells, with a 6-fold reduction in multipolar anaphases (Figures 4B and 4C). A similar result was observed by live imaging (Figures 4D and 4E), with no delay in mitosis (Figure 4F).

Next, to examine how PP2A-A$\alpha^{P179R/+}$ cells cluster centrosomes more efficiently, we asked if microtubule organization in mitosis is more robust in PP2A-A$\alpha^{P179R/+}$ cells. Although centrosomes are the major sites of microtubule nucleation, a bipolar spindle can assemble in the absence of one or both centrosomes, albeit with some delay (Khodjakov et al., 2000). We generated acentrosomal cells using centrinone, a small-molecule inhibitor of Plk4 (Wong et al., 2015) and measured the time between nuclear envelope breakdown and anaphase onset by live imaging. WT and PP2A-A$\alpha^{P179R/+}$ cells were similarly delayed upon centrinone treatment (Figures S2G and S2H), indicating that spindle assembly is not more robust in acentrosomal PP2A-A$\alpha^{P179R/+}$ cells. Spindle positioning and centrosome clustering in mitosis depends on cortical forces

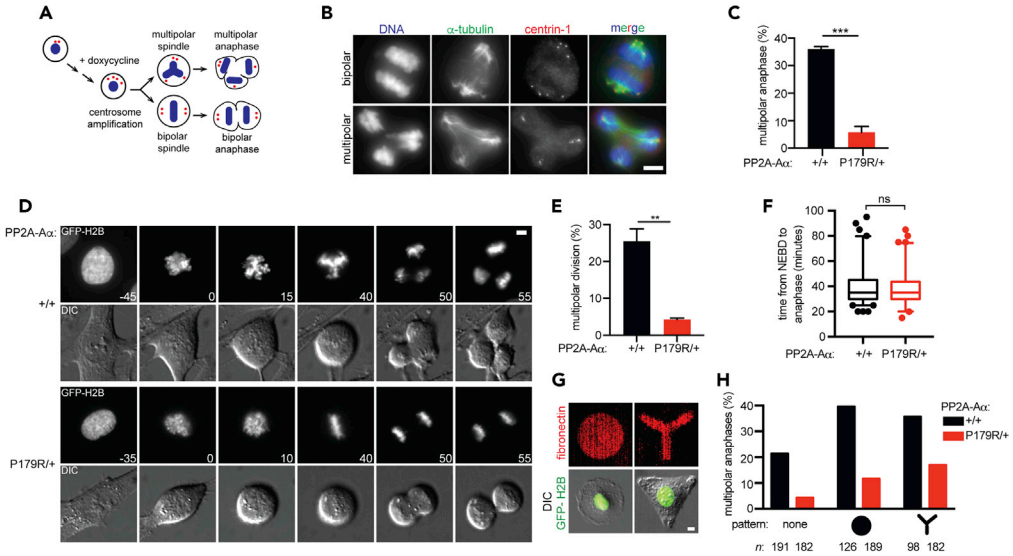

Figure 4. PP2A-Aα$^{P179R/+}$ Cells Exhibit More Robust Centrosome Clustering

(A) Schematic of centrosome amplification induction by doxycycline (dox)-inducible Plk4 overexpression.

(B and C) Plk4-inducible cells were treated with dox and fixed and analyzed by immunofluorescence. (B) Representative bipolar (top) and multipolar (bottom) anaphases. (C) Multipolar anaphase incidence in cells with >4 centrin-1 foci is plotted.

(D–F) Plk4-inducible cells were treated with dox and imaged live (D) GFP-H2B (top) and differential interference contrast (bottom) montage. Time (minutes) relative to nuclear envelope breakdown is indicated. (E) Incidence of multipolar cell division is plotted. (F) A box-and-whisker plot of mitotic duration in dox-treated cells undergoing bipolar cell divisions. Whiskers indicate the 5th–95th percentile range, and circles indicate cells outside of this range. Result is representative of three experiments.

(G and H) Plk4-inducible cells were treated with dox and imaged on O- and Y-shaped fibronectin micro-patterns. (G) Representative images of interphase cells. (H) Incidence of multipolar anaphases. *n*, total cells analyzed.

(C and E) Mean ± SEM from three experiments. Scale bars, 5 μm. ***$p < 0.0005$, **$p < 0.005$; ns, not significant ($p > 0.05$) Student's t test.

See also Figure S2.

and interphase cell shape (Kwon et al., 2015; Rhys et al., 2018; Théry et al., 2005). To examine the contribution of cortical forces to spindle positioning, cells were plated on L-shaped fibronectin micro-patterned coverslips. Spindle positioning was not impaired in PP2A-Aα$^{P179R/+}$ cells with two centrosomes (Figures S2I–S2K). We next examined the contribution of cortical forces and interphase cell shape to centrosome clustering in PP2A-Aα$^{P179R/+}$ cells. Centrosome amplification was induced by Plk4 overexpression and cells plated onto O- or Y-shaped fibronectin micro-patterns (Figure 4G, S2L, and S2M). Both shapes bias cells with supernumerary centrosomes toward multipolar cell divisions (Kwon et al., 2008). Indeed, in WT cells these patterns resulted in 1.8-fold and 1.6-fold increases in the frequency of multipolar cell divisions on O- and Y- shaped patterns, respectively (Figure 4H). Interestingly, in PP2A-Aα$^{P179R/+}$ cells the frequency of multipolar cell divisions was increased by 2.6- and 3.9-fold on O- and Y- shaped patterns, respectively (Figure 4H). Thus, centrosome clustering efficiency in PP2A-Aα$^{P179R/+}$ cells is more sensitive to interphase cell shape compared with WT cells. However, the overall frequency of multipolar cell divisions in PP2A-Aα$^{P179R/+}$ cells was still reduced compared with WT cells (Figure 4H) suggesting that although cortical forces contribute to enhanced centrosome clustering in PP2A-Aα$^{P179R/+}$ cells, the phenotype likely also arises from mechanisms unrelated to cell shape.

DISCUSSION

Human tumors frequently have centrosome amplification (Chan, 2011), and cancer cells tend to be more proficient at clustering supernumerary centrosomes (Ganem et al., 2009). Thus, in addition to relying on the intrinsic centrosome clustering ability of cells (Drosopoulos et al., 2014; Kwon et al., 2008, 2015; Leber et al., 2010; Quintyne et al., 2005), cancer cells may acquire mutations that improve clustering efficiency. Here we have characterized a hotspot P179R mutation in PP2A-Aα that allows cells to cluster supernumerary centrosomes more efficiently. This finding is important because cells with supernumerary centrosomes

only survive mitosis if they cluster centrosomes (Ganem et al., 2009). Our data suggest that a potential explanation for the enrichment of *PPP2R1A* mutations in tumors that experience WGD is to allow cells to survive the mitotic stress associated with centrosome amplification. Tolerance to WGD has been shown to confer chromosomal instability and promote tumor genome evolution and is linked to poor prognosis (Bielski et al., 2018; Dewhurst et al., 2014). Therefore, cancer-associated mutations in PP2A-Aα could also serve as a prognostic marker of tumor progression and is in agreement with *PPP2R1A* being annotated as a cancer driver in gynecological tumors (Bailey et al., 2018).

Our findings also highlight the importance of considering PP2A-Aα mutations in a context that closely resembles the genetic change in tumors and suggest that the enhanced centrosome clustering efficiency arises from haploinsufficiency in PP2A-Aα function. Interestingly, the reduction in PP2A functionality by the P179R mutation in PP2A-Aα has been identified as a driver of tumorigenesis in uterine cancers (Taylor et al., 2019) and is consistent with the known tumor suppressor role of PP2A (Pallas et al., 1990). Therefore, if the primary impact of the mutation is to reduce PP2A-Aα functionality, then it is perhaps unexpected that missense mutations dominate the *PPP2R1A* mutational landscape rather than truncations. Considering the heterotrimeric structure of PP2A holoenzymes, it is possible that several essential functions of PP2A may still be fulfilled by the mutant PP2A-Aα, including association with the catalytic subunit and association with STRN regulatory subunits, neither of which was altered by the P179R or R183W mutation. Thus the mutations may selectively impact the subset of PP2A holoenzymes with tumor suppressor functions. Given that small-molecule activators of PP2A have been shown to reduce the tumorigenicity associated with PP2A inactivation by the P179R mutation (Taylor et al., 2019), it will be important to further investigate the anti-tumor efficacies of pharmacologic activators of PP2A (Ramaswamy et al., 2015; Sangodkar et al., 2017) in human cancers with other oncogenic PP2A mutations.

Furthermore, our work reveals that decreasing PP2A functionality increases centrosome clustering. This observation together with the identification of a role for PP2A-B55/SUR-6 in regulating centrosome separation during mitotic entry (Boudreau et al., 2019) opens new avenues of exploration for a role of PP2A in the regulation of centrosome clustering. Our data also suggest that fine-tuning phosphoregulation, in the form of a heterozygous PP2A-Aα mutation, allows a human cell to become more proficient at centrosome clustering without compromising mitotic fidelity. Because the mutation only partially reduces PP2A-Aα function, and a WT allele remains present in the cell, we predict that the observed phenotype is due to small changes in phosphorylation of substrates that impact centrosome positioning and engagement during mitosis. Therefore, future work will focus on characterizing phosphorylation sites that control centrosome clustering in PP2A-Aα$^{P179R/+}$ cells.

Limitations of the Study

One limitation of this study is that we examined the impact of PP2A-Aα mutations in a non-cancer cell line. The advantage of this choice is that we could determine that the mutation is sufficient to alter centrosome clustering, whereas the limitation is that we did not examine the mutation in a transformed cell. The other limitation is that we did not perform gene replacement for all PP2A-Aα isoforms, and therefore further studies are needed to determine if this effect on centrosome clustering is shared among other recurrent mutations.

METHODS

All methods can be found in the accompanying Transparent Methods supplemental file.

SUPPLEMENTAL INFORMATION

Supplemental Information can be found online at https://doi.org/10.1016/j.isci.2019.07.018.

ACKNOWLEDGMENTS

We thank Veronica Rodriguez-Bravo and Sun Joo Lee for experimental assistance and Prasad Jallepalli and Bryan Tsou for helpful discussions. This work was supported by the Functional Genomics Initiative at Memorial Sloan Kettering (E.A.F. and A.K.), NIH/NIGMS GM125996 (E.A.F), and NCI CA214812 to A.K. This work was prepared while E.A.F. was employed at Memorial Sloan Kettering Cancer Center. The opinions expressed in this article are the author's own and do not reflect the view of the National Institutes of Health, the Department of Health and Human Services, or the US government.

AUTHOR CONTRIBUTIONS

Formal analysis and investigation, N.V.A., M.M.-O., and P.C.; Conceptualization, experiment design, and writing, N.V.A. and E.A.F.; Funding acquisition, E.A.F. and A. K.

DECLARATION OF INTERESTS

The authors declare no competing interests.

Received: May 6, 2019
Revised: June 27, 2019
Accepted: July 12, 2019
Published: September 27, 2019

REFERENCES

Andreassen, P.R., Lohez, O.D., Lacroix, F.B., and Margolis, R.L. (2001). Tetraploid state induces p53-dependent arrest of nontransformed mammalian cells in G1. Mol. Biol. Cell *12*, 1315–1328.

Bailey, M.H., Tokheim, C., Porta-Pardo, E., Sengupta, S., Bertrand, D., Weerasinghe, A., Colaprico, A., Wendl, M.C., Kim, J., Reardon, B., et al. (2018). Comprehensive characterization of cancer driver genes and mutations. Cell *173*, 371–385.e18.

Basto, R., Brunk, K., Vinadogrova, T., Peel, N., Franz, A., Khodjakov, A., and Raff, J.W. (2008). Centrosome amplification can initiate tumorigenesis in flies. Cell *133*, 1032–1042.

Berdougo, E., Terret, M.-E., and Jallepalli, P.V. (2009). Functional dissection of mitotic regulators through gene targeting in human somatic cells. Methods Mol. Biol. *545*, 21–37.

Bielski, C.M., Zehir, A., Penson, A.V., Donoghue, M.T.A., Chatila, W., Armenia, J., Chang, M.T., Schram, A.M., Jonsson, P., Bandlamudi, C., et al. (2018). Genome doubling shapes the evolution and prognosis of advanced cancers. Nat. Genet. *50*, 1189–1195.

Boudreau, V., Chen, R., Edwards, A., Sulaimain, M., and Maddox, P.S. (2019). PP2A-B55/SUR-6 collaborates with the nuclear lamina for centrosome separation during mitotic entry. Mol. Biol. Cell *30*, 876–886.

Carter, S.L., Cibulskis, K., Helman, E., McKenna, A., Shen, H., Zack, T., Laird, P.W., Onofrio, R.C., Winckler, W., Weir, B.A., et al. (2012). Absolute quantification of somatic DNA alterations in human cancer. Nat. Biotechnol. *30*, 413–421.

Cerami, E., Gao, J., Dogrusoz, U., Gross, B.E., Sumer, S.O., Aksoy, B.A., Jacobsen, A., Byrne, C.J., Heuer, M.L., Larsson, E., et al. (2012). The cBio cancer genomics portal: an open platform for exploring multidimensional cancer genomics data. Cancer Discov. *2*, 401–404.

Chan, J.Y. (2011). A clinical overview of centrosome amplification in human cancers. Int. J. Biol. Sci. *7*, 1122–1144.

Chen, W., Possemato, R., Campbell, K.T., Plattner, C.A., Pallas, D.C., and Hahn, W.C. (2004). Identification of specific PP2A complexes involved in human cell transformation. Cancer Cell *5*, 127–136.

Cho, U.S., and Xu, W. (2007). Crystal structure of a protein phosphatase 2A heterotrimeric holoenzyme. Nature *445*, 53–57.

Cooper, J.A. (1987). Effects of cytochalasin and phalloidin on actin. J. Cell Biol. *105*, 1473–1478.

Craney, A., Kelly, A., Jia, L., Fedrigo, I., Yu, H., and Rape, M. (2016). Control of APC/C-dependent ubiquitin chain elongation by reversible phosphorylation. Proc. Natl. Acad. Sci. U. S. A *113*, 1540–1545.

Cuenda, A., Rouse, J., Doza, Y.N., Meier, R., Cohen, P., Gallagher, T.F., Young, P.R., and Lee, J.C. (1995). SB 203580 is a specific inhibitor of a MAP kinase homologue which is stimulated by cellular stresses and interleukin-1. FEBS Lett. *364*, 229–233.

Dewhurst, S.M., McGranahan, N., Burrell, R.A., Rowan, A.J., Grönroos, E., Endesfelder, D., Joshi, T., Mouradov, D., Gibbs, P., Ward, R.L., et al. (2014). Tolerance of whole-genome doubling propagates chromosomal instability and accelerates cancer genome evolution. Cancer Discov. *4*, 175–185.

Drosopoulos, K., Tang, C., Chao, W.C.H., and Linardopoulos, S. (2014). APC/C is an essential regulator of centrosome clustering. Nat. Commun. *5*, 3686.

Espert, A., Uluocak, P., Bastos, R.N., Mangat, D., Graab, P., and Gruneberg, U. (2014). PP2A-B56 opposes Mps1 phosphorylation of Knl1 and thereby promotes spindle assembly checkpoint silencing. J. Cell Biol. *206*, 833–842.

Foley, E.A., Maldonado, M., and Kapoor, T.M. (2011). Formation of stable attachments between kinetochores and microtubules depends on the B56-PP2A phosphatase. Nat. Cell Biol. *13*, 1265–1271.

Ganem, N.J., Godinho, S.A., and Pellman, D. (2009). A mechanism linking extra centrosomes to chromosomal instability. Nature *460*, 278–282.

Gao, J., Aksoy, B.A., Dogrusoz, U., Dresdner, G., Gross, B., Sumer, S.O., Sun, Y., Jacobsen, A., Sinha, R., Larsson, E., et al. (2013). Integrative analysis of complex cancer genomics and clinical profiles using the cBioPortal. Sci. Signal. *6*, pl1.

Haesen, D., Abbasi Asbagh, L., Derua, R., Hubert, A., Schrauwen, S., Hoorne, Y., Amant, F., Waelkens, E., Sablina, A., and Janssens, V. (2016). Recurrent PPP2R1A mutations in uterine cancer act through a dominant-negative mechanism to promote malignant cell growth. Cancer Res. *76*, 5719–5731.

Hertz, E.P.T., Kruse, T., Davey, N.E., López-Méndez, B., Sigurðsson, J.O., Montoya, G., Olsen, J.V., and Nilsson, J. (2016). A Conserved motif provides binding specificity to the PP2A-B56 phosphatase. Mol. Cell *63*, 686–695.

Hyodo, T., Ito, S., Asano-Inami, E., Chen, D., and Senga, T. (2016). A regulatory subunit of protein phosphatase 2A, PPP2R5E, regulates the abundance of microtubule crosslinking factor 1. FEBS J. *283*, 3662–3671.

Jeong, A.L., Han, S., Lee, S., Su Park, J., Lu, Y., Yu, S., Li, J., Chun, K.-H., Mills, G.B., and Yang, Y. (2016). Patient derived mutation W257G of PPP2R1A enhances cancer cell migration through SRC-JNK-c-Jun pathway. Sci. Rep. *6*, 27391.

Khodjakov, A., Cole, R.W., Oakley, B.R., and Rieder, C.L. (2000). Centrosome-independent mitotic spindle formation in vertebrates. Curr. Biol. *10*, 59–67.

Kitajima, T.S., Sakuno, T., Ishiguro, K., Iemura, S., Natsume, T., Kawashima, S.A., and Watanabe, Y. (2006). Shugoshin collaborates with protein phosphatase 2A to protect cohesin. Nature *441*, 46–52.

Kleylein-Sohn, J., Westendorf, J., Le Clech, M., Habedanck, R., Stierhof, Y.-D., and Nigg, E.A. (2007). Plk4-induced centriole biogenesis in human cells. Dev. Cell *13*, 190–202.

Kwon, M., Godinho, S.A., Chandhok, N.S., Ganem, N.J., Azioune, A., Thery, M., and Pellman, D. (2008). Mechanisms to suppress multipolar divisions in cancer cells with extra centrosomes. Genes Dev. *22*, 2189–2203.

Kwon, M., Bagonis, M., Danuser, G., and Pellman, D. (2015). Direct microtubule-binding by myosin-10 orients centrosomes toward retraction fibers and subcortical actin clouds. Dev. Cell *34*, 323–337.

Leber, B., Maier, B., Fuchs, F., Chi, J., Riffel, P., Anderhub, S., Wagner, L., Ho, A.D., Salisbury, J.L., Boutros, M., et al. (2010). Proteins required for centrosome clustering in cancer cells. Sci. Transl. Med. *2*, 33ra38.

Lee, S.J., Rodriguez-Bravo, V., Kim, H., Datta, S., and Foley, E.A. (2017). The PP2A ^{B56} phosphatase

promotes the association of Cdc20 with APC/C in mitosis. J. Cell Sci. *130*, 1760–1771.

Nijenhuis, W., Vallardi, G., Teixeira, A., Kops, G.J., and Saurin, A.T. (2014). Negative feedback at kinetochores underlies a responsive spindle checkpoint signal. Nat. Cell Biol. *16*, 1257–1264.

Pallas, D.C., Shahrik, L.K., Martin, B.L., Jaspers, S., Miller, T.B., Brautigan, D.L., and Roberts, T.M. (1990). Polyoma small and middle T antigens and SV40 small t antigen form stable complexes with protein phosphatase 2A. Cell *60*, 167–176.

Peel, N., Stevens, N.R., Basto, R., and Raff, J.W. (2007). Overexpressing centriole-replication proteins in vivo induces centriole overduplication and de novo formation. Curr. Biol. *17*, 834–843.

Quintyne, N.J., Reing, J.E., Hoffelder, D.R., Gollin, S.M., and Saunders, W.S. (2005). Spindle multipolarity is prevented by centrosomal clustering. Science *307*, 127–129.

Ramaswamy, K., Spitzer, B., and Kentsis, A. (2015). Therapeutic re-activation of protein phosphatase 2A in acute myeloid leukemia. Front. Oncol. *5*, 16.

Rhys, A.D., Monteiro, P., Smith, C., Vaghela, M., Arnandis, T., Kato, T., Leitinger, B., Sahai, E., McAinsh, A., Charras, G., et al. (2018). Loss of E-cadherin provides tolerance to centrosome amplification in epithelial cancer cells. J. Cell Biol. *217*, 195–209.

Ring, D., Hubble, R., and Kirschner, M. (1982). Mitosis in a cell with multiple centrioles. J. Cell Biol. *94*, 549–556.

Sangodkar, J., Perl, A., Tohme, R., Kiselar, J., Kastrinsky, D.B., Zaware, N., Izadmehr, S., Mazhar, S., Wiredja, D.D., O'Connor, C.M., et al. (2017). Activation of tumor suppressor protein PP2A inhibits KRAS-driven tumor growth. J. Clin. Invest. *127*, 2081–2090.

Schmitz, M.H.A., Held, M., Janssens, V., Hutchins, J.R.A., Hudecz, O., Ivanova, E., Goris, J., Trinkle-Mulcahy, L., Lamond, A.I., Poser, I., et al. (2010). Live-cell imaging RNAi screen identifies PP2A–B55α and importin-β1 as key mitotic exit regulators in human cells. Nat. Cell Biol. *12*, 886–893.

Straight, A.F., Cheung, A., Limouze, J., Chen, I., Westwood, N.J., Sellers, J.R., and Mitchison, T.J. (2003). Dissecting temporal and spatial control of cytokinesis with a myosin II inhibitor. Science *299*, 1743–1747.

Taylor, Sarah E., O'Connor, C.M., Wang, Z., Shen, G., Song, H., Leonard, D., Sangodkar, J., LaVasseur, C., Avril, S., Waggoner, S., et al. (2019). The highly recurrent PP2A Aα-subunit mutation P179R alters protein structure and impairs PP2A enzyme function to promote endometrial tumorigenesis. Cancer Res. https://doi.org/10.1158/0008-5472.CAN-19-0218.

Théry, M., Racine, V., Pépin, A., Piel, M., Chen, Y., Sibarita, J.-B., and Bornens, M. (2005). The extracellular matrix guides the orientation of the cell division axis. Nat. Cell Biol. *7*, 947–953.

Wang, W.J., Soni, R.K., Uryu, K., and Tsou, M.F.B. (2011). The conversion of centrioles to centrosomes: essential coupling of duplication with segregation. J. Cell Biol. *193*, 727–739.

Wong, Y.L., Anzola, J.V., Davis, R.L., Yoon, M., Motamedi, A., Kroll, A., Seo, C.P., Hsia, J.E., Kim, S.K., Mitchell, J.W., et al. (2015). Reversible centriole depletion with an inhibitor of Polo-like kinase 4. Science *348*, 1155–1160.

Xu, Y., Xing, Y., Chen, Y., Chao, Y., Lin, Z., Fan, E., Yu, J.W., Strack, S., Jeffrey, P.D., and Shi, Y. (2006). Structure of the protein phosphatase 2A holoenzyme. Cell *127*, 1239–1251.

Xu, Y., Chen, Y., Zhang, P., Jeffrey, P.D., and Shi, Y. (2008). Structure of a protein phosphatase 2A holoenzyme: insights into B55-mediated Tau dephosphorylation. Mol. Cell *31*, 873–885.

Yang, Z., Lončarek, J., Khodjakov, A., and Rieder, C.L. (2008). Extra centrosomes and/or chromosomes prolong mitosis in human cells. Nat. Cell Biol. *10*, 748–751.

Zack, T.I., Schumacher, S.E., Carter, S.L., Cherniack, A.D., Saksena, G., Tabak, B., Lawrence, M.S., Zhang, C.-Z., Wala, J., Mermel, C.H., et al. (2013). Pan-cancer patterns of somatic copy number alteration. Nat. Genet. *45*, 1134–1140.

Zhou, J., Pham, H.T., Ruediger, R., and Walter, G. (2003). Characterization of the Aalpha and Abeta subunit isoforms of protein phosphatase 2A: differences in expression, subunit interaction, and evolution. Biochem. J. *369*, 387–398.

ISCI, Volume *19*

Supplemental Information

A Cancer-Associated Missense Mutation in PP2A-Aα Increases Centrosome Clustering during Mitosis

Noelle V. Antao, Marina Marcet-Ortega, Paolo Cifani, Alex Kentsis, and Emily A. Foley

SUPPLEMENTAL INFORMATION TITLES AND LEGENDS

Figure S1. Analysis of PP2A activity and holoenzyme assembly in PP2A-Aα$^{P179R/+}$ cells, Related to Figure 2. (A-B) PP2A-Aα IPs in mitotic lysates from WT (+/+) or PP2A-Aα$^{P179R/+}$ (P179R/+). Okadaic acid was included in wash steps as indicated. The reaction was split and **(A)** associated proteins were analyzed by western blot or **(B)** incubated with a phosphopeptide substrate. Phosphate release was quantified using a molybdate dye-based spectrophotometric assay. Absorbance values were normalized to the maximum value per experiment. Mean ± s.d. from three experiments is plotted. **(C)** Plotted is the normalized mean ± s.e.m. of the amount of bait protein (PP2A-Aα) IP'd in the experiment in Figure 2D performed at least three times. **(D)** Western blot analysis of lysates (lanes 1-2) and IPs of control IgG (lane 3) or PP2A-Aα IgG (lane 4-5) in indicated cell lines **(E)** Plotted is the normalized mean ± s.e.m. of the experiment in (D) performed three times. a.u., arbitrary units. ****, $P < 0.00005$, ***, $P < 0.0005$, ns, not significant ($P > 0.05$) Student's *t*-test

Figure S2. Analysis of mitotic duration in PP2A-Aα$^{P179R/+}$ cells and centrosome amplification efficiency in Plk4-inducible cells, Related to Figure 3 and 4 (A) WT (+/+) and PP2A-Aα$^{P179R/+}$ (P179R/+) cells were imaged live and the time from nuclear envelope breakdown to anaphase onset was measured. Clones a and b are independently derived cell lines. A box-and-whisker plot is shown. Whiskers indicate the 5-95 percentile range and circles indicate cells outside of this range. Result is representative of two experiments. **(B)** Maximum intensity projections of WT (+/+) and PP2A-Aα$^{P179R/+}$ (P179R/+) cells treated with cytochalasin D and then briefly with nocodazole. Cells were analyzed for microtubule re-growth by immunofluorescence upon nocodazole removal. **(C-D)** Cells were treated with cytochalasin D, fixed and analyzed by immunofluorescence. **(C)** Representative maximum intensity projection. **(D)** Multipolar anaphase incidence in cells with four centrin-1 foci is plotted (mean ± s.e.m. of the experiment in (C) performed three times). **(E-F)** *Tp53*$^{-/-}$ WT (+/+) and PP2A-Aα$^{P179R/+}$ (P179R/+) cells with tet-inducible Plk4 expression were treated with dox or DMSO for 30 h, arrested in G2 with RO-3306 and dox or DMSO for 18 h, fixed and processed for

immunofluorescence. **(E)** Maximum intensity projections of C-Nap1 and a merge with centrin-1 and DNA. **(F)** Fraction of cells with >2 centrosomes (mean ± s.d. from two experiments with 200 cells scored per condition, per experiment). **(G-H)** Cells were imaged live after DMSO or centrinone treatment. **(G)** RFP-H2B montage of centrinone treated cells. Time (min) relative to nuclear envelope breakdown is indicated. **(H)** Mitotic duration is plotted. Line, median; circle, cell. Result is representative of three experiments **(I-K)** Cell division on L-shaped fibronectin micro-patterns in cells with two centrosomes. **(I)** Schematic of cell division on an L-shaped fibronectin pattern (grey). The angle (α) of chromosome segregation axis (solid line) relative to the reference X-axis (dashed line) is measured. Chromatin, green; Centrosome, red. **(J)** GFP-H2B and DIC merge time-lapse images. Time (min) relative to nuclear envelope breakdown is indicated. **(K)** Percentage of cells dividing within 30 degrees of the median angle is plotted (mean ± s.d. of two experiments). **(L-M)** GFP-H2B and DIC merge time-lapse images of Plk4-inducible cells treated with dox and imaged on (L) O-shaped and (M) Y-shaped fibronectin micro-patterns. Time (min) relative to nuclear envelope breakdown is indicated. Scale bars, 5 μm. ****, $P < 0.00005$, **, $P < 0.005$, *, $P < 0.05$, ns, not significant ($P > 0.05$) Student's *t*-test.

Antao et al. Figure S1, Related to Figure 2

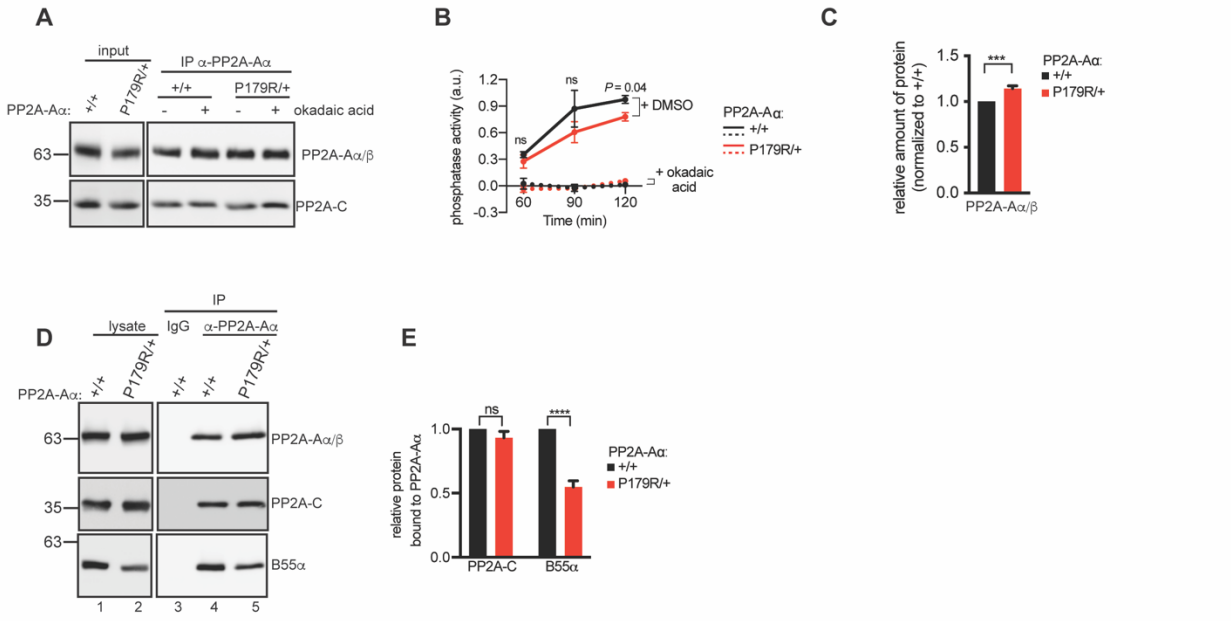

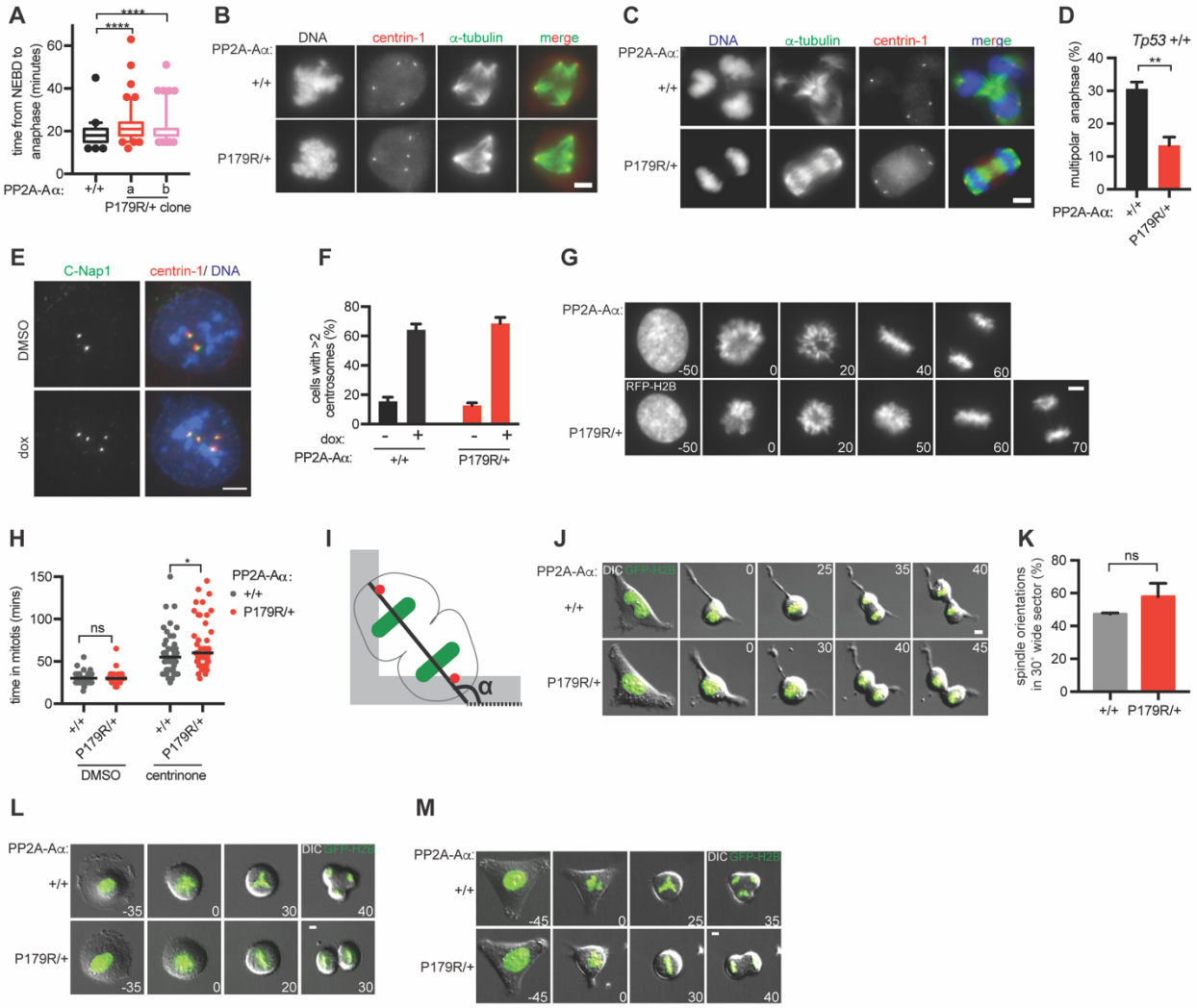
A
time from NEBD to anaphase (minutes)
PP2A-Aα:
+/+
a
b
P179R/+ clone
B
DNA
centrin-1
α-tubulin
merge
PP2A-Aα:
+/+
P179R/+
C
DNA
α-tubulin
centrin-1
merge
PP2A-Aα:
+/+
P179R/+
D
Tp53 +/+
multipolar anaphsae (%)
PP2A-Aα:
+/+
P179R/+
E
C-Nap1
centrin-1/ DNA
DMSO
dox
F
cells with >2 centrosomes (%)
dox:
PP2A-Aα:
+/+
P179R/+
G
PP2A-Aα:
RFP-H2B
P179R/+
H
time in mitotis (mins)
PP2A-Aα:
+/+
P179R/+
ns
DMSO
centrinone
I
α
J
PP2A-Aα:
DIC GFP-H2B
+/+
P179R/+
K
spindle orientations in 30˚ wide sector (%)
ns
+/+
P179R/+
L
PP2A-Aα:
DIC GFP-H2B
+/+
P179R/+
M
PP2A-Aα:
DIC GFP-H2B
+/+
P179R/+

TRANSPARENT METHODS

Contact for reagent and resource sharing

Further information and requests for resources and reagents should be directed to and will be fulfilled by the Lead Contact, Emily A Foley (emilyafoley@gmail.com).

Experimental model and subject details

RPE-1 hTERT (WT) cells (a gift from Alexey Khodjakov) and derivative cell lines were grown at 37°C in a humidified atmosphere with 5% CO_2 in DMEM:F12 growth medium. Human embryonic kidney 293-T cells (ATCC) and Human embryonic kidney 293 cells (ATCC) were grown in DMEM growth medium. All media were supplemented with 10% fetal bovine serum (VWR Life Science), penicillin-streptomycin (Gemini Bio-Products), non-essential amino acids (Life Technologies), and L-glutamine (Sigma-Aldrich). Cell lines were authenticated upon initial receipt and upon initial generation by Short Tandem Repeat analysis at the Integrated Genomics Operations at Memorial Sloan Kettering Cancer Center. Cell lines were also tested for mycoplasma contamination by the Antibody and Bioresource core facility at Memorial Sloan Kettering Cancer Center.

Cell line generation

To generate the PP2A-A$\alpha^{P179R/+}$ cell lines, we used adeno-associated virus-mediated gene targeting. Q5 High-Fidelity DNA polymerase (New England Biolabs) was used to amplify two homology arms spanning exons 5 and 6 of *PPP2R1A* and cloned into a bacterial artificial chromosome (Life Technologies). The homology arms were cloned into vector pNX (Papi et al., 2005) flanking a *loxP*-Neo^R-*loxP* cassette. Site-directed mutagenesis was used to introduce a C to G mutation at nucleotide 23280 in exon 5 of *PPP2R1A*. The *PPP2R1A* homology fragment was then cloned into pAAV (Berdougo et al., 2009) by NotI restriction enzyme digestion. Isolation of AAV particles, selection of stable transductants, and PCR screening were carried out as previously described (Berdougo et al., 2009). We determined the *PPP2R1A* genotype in isolated clones by genomic PCR amplification of *PPP2R1A* followed by Sanger sequencing. We isolated two clones (termed a and b), each with a heterozygous *PPP2R1A* P179R mutation. For

each clone, the neomycin cassette was excised by infecting cells with adenovirus expressing Cre recombinase (Vector Development Laboratory, Baylor College of Medicine) at a multiplicity of infection of 80 plaque-forming units/cell. We identified single clones that were negative for the neomycin cassette but positive for the remnant loxP site by PCR amplification of endogenous *PPP2R1A*. Clone a was used for all experiments and, where indicated, clone b was also examined.

To generate *Tp53* knockout cell lines, codon-optimized Cas9 (Addgene 41815) and a guide RNA targeting *Tp53* (Wang et al., 2015) were transfected into cells using a Nucleofector 2b Device (Lonza) with the setting T023. Colonies were screened for p53 loss by western blot using an antibody for the N-terminus of p53 (Santa Cruz Biotechnology SC-126, clone DO-1). To generate cell lines expressing tetracycline-inducible Plk4, we used the lentiviral pLVX-Tight-Puro system (Clontech). Lentiviruses were generated in HEK 293T cells transfected with psPAX2 (Addgene plasmid 12260), pCMV-VSV-G (Addgene plasmid 8454) and Plk4 cloned into pLVX-Tight-puro (Clontech) using Lipofectamine 2000 (Thermo Fisher Scientific) according to manufacturer's instructions. 48 h after transfection, the virus containing suspension from HEK293T cells was filtered with a 0.45 μM filter (EMD Millipore), supplemented with polybrene (4 μg/mL, Sigma) and applied to *Tp53*-knockout WT cells or PP2A-Aα$^{P179R/+}$ cells. Cells were first transduced with Plk4 in pLVX-tight-puro lentivirus and selected with puromycin (15 μg/mL, Thermo Fisher Scientific) for 1 week. Puromycin-resistant cells were then grown in Tetracycline-free serum (Clontech) and transduced with pLVX-Tet-On-Advanced lentivirus followed by G418 selection (500 μg/mL, Thermo Fisher Scientific) for 1 week. For each PP2A-Aα genotype, we chose a clone that yielded centrosome amplification in 60% of cells after 48 h doxycycline treatment (1 μg/mL).

We generated cells with fluorescent H2B by lentiviral transduction. H2B-RFP (Addgene plasmid 26001) or H2B-GFP (Addgene plasmid 25999) plasmids were co-transfected with psPAX2 and pCMV-VSV-G into HEK 293T cells. Supernatants were filtered, mixed with polybrene (4 μg/mL) and applied to target cells. We generated cells expressing GFP-PP2Aα by retroviral transduction as in (Foley et al., 2011) using WT PP2A-Aα (Foley et

al., 2011) or P179R and R183W mutants, which were cloned via site-directed mutagenesis.

Inhibitor treatments

Commercially available small molecules and chemical inhibitors were used as follows - cytochalasin D (0.2 μM), cytochalasin B (4 μM), blebbistatin (100 μM), SB203580 (10 μM), doxycycline (1 μg/mL), nocodazole (3.3 μM), centrinone (200 nM), and Okadaic acid (200 nM). To induce whole genome doubling, cells were plated in a glass bottom dish (Cellvis) or on coverslips (Fisher) and, 24 h later, treated with cytochalasin D, cytochalasin B, or blebbistatin for 20 h. To wash out the inhibitor, the media was replaced six times over 1 h. *Tp53*$^{+/+}$ cells were released into SB203580, and imaged 20 h later. This inhibitor was omitted in *Tp53*$^{-/-}$ cells. Cells were then fixed and processed for immunofluorescence microscopy or imaged live by DIC and fluorescence microscopy. Plk4 induction with doxycycline was performed for 48 h. Unless otherwise indicated, ≥50 cells were analyzed per condition, per experiment and at least three experiments were analyzed per treatment condition. Where indicated, mitotic cell enrichment was performed using a 14 h treatment with nocodazole followed by manual detachment from the tissue culture dish.

Live-cell imaging

Live imaging was performed on a Nikon Eclipse TiE inverted microscope equipped with a PI Piezo stage controller and Nikon Perfect Focus. Cells were maintained at 37 °C and 5% CO_2 with a Stage Top Incubator with Flow Control and a Sub Stage Environmental Enclosure (Tokai Hit). Cells were imaged by DIC and fluorescence microscopy (GFP-Ex470 nm; Em522 nm or DsRed-Ex508 nm; Em620 nm). Images were acquired with a 20X or 40X objective and recorded on a deep-cooled, ultra-low noise sCMOS camera (Andor) at 16-bit depth using Elements software (Nikon). Image cropping was performed in Fiji (Schindelin et al., 2012).

Immunofluorescence microscopy

For immunofluorescence microscopy of α-tubulin, C-Nap 1, and centrin-1, cells on coverslips were fixed in methanol at −20 °C for 10 min. For PP2A-Aα and B56α

immunofluorescence, cells on coverslips were pre-extracted for 40 s at 37 °C in PEM buffer (100 mM K-PIPES pH 6.9, 10 mM EGTA, 1 mM $MgCl_2$) with 0.5% Triton X-100 and 4 M glycerol. Coverslips were then fixed in PEM buffer with 3.7% formaldehyde and 0.2% Triton X-100 for 5 min at 37 °C. Coverslips were washed in TBS + 0.1% Triton X-100, blocked in same buffer with 2% donkey serum (Jackson Immunoresearch Laboratories) for 30 min, and stained with primary antibody for 3 h at room temperature. Species-specific secondary antibodies conjugated to Alexa Fluor 488, Rhodamine, Alexa Fluor 647 (Jackson Immunoresearch Laboratories), or IgG2a Alexa Fluor 594 (Thermo Fisher Scientific) were applied for 30 min at 0.6 µg/mL. Coverslips were mounted onto slides with Prolong Gold with DAPI (Thermo Fisher Scientific) and sealed. Imaging was performed on a DeltaVision Elite microscope running softWoRx software (GE Life Sciences). Images were acquired at 60X or 100X magnification with a PCO Edge CMOS Camera. Z-stacks were acquired with 0.2 µm spacing. Maximum intensity projection images were created in softWoRx. Pseudo coloring and cropping was performed in Fiji (Schindelin et al., 2012) and images were assembled in Illustrator (Adobe, San Jose, CA). Kinetochore/centromere intensity was calculated in Fiji using published analysis macros (Nijenhuis et al., 2014). 20 cells were analyzed per condition per experiment.

Antibodies

Primary antibodies were used at 1 µg/mL for immunofluorescence incubations and 0.1 µg/mL for western blotting incubations. 2-4 µg of IgG was used for immunoprecipitation. Custom PP2A-Aα antibody was generated by immunizing rabbits with the peptide sequence of MAAADGDDSLY conjugated to matriculture Keyhole Limpet Hemocyanin (Thermo Scientific). Antigens were injected into New Zealand White rabbits using an institutionally approved protocol and animal-care facility (Pocono Rabbit Farm and Laboratory, Canadensis, PA). To purify peptide antibodies, antisera were diluted with 0.1 vol 10X PBS and incubated overnight with immunizing peptide covalently coupled to sulfo-link resin (Thermo Fisher Scientific). After washing with PBS, antibodies were eluted with 0.2 M glycine, pH 2.5 and subsequently neutralized with Tris pH 8.0, followed by dialysis into PBS. Custom GFP antibodies were raised against bacterially expressed GST-GFP. The serum was loaded onto a HiTrap NHS-activated HP column (GE Life

Sciences) coupled to GST-GFP. Commercial and published antibodies used in this study include: B56α (immunofluorescence: BD Biosciences, 610615; western (Lee et al., 2017)), B56γ (Bethyl Laboratories, A303-814A), B56δ (Bethyl Laboratories, A301-100A), B56ε (Lee et al., 2017), B55α (Santa Cruz Biotechnology, SC-81606), PP2A-Aα/β (Santa Cruz Biotechnology, SC-6112), PP2A-C (BD Biosciences, 610555), centrin-1 (EMD Millipore, 04-1624), CREST Serum (Immunovision, HCT-0100; used at 1:5,000 dilution), α-tubulin (mouse DM1α; Abcam, ab7291), α-tubulin FITC conjugated (Sigma F2168), β-actin (Santa Cruz Biotechnology, SC-47778), p53 (Santa Cruz Biotechnology SC-126, clone DO-1), and C-Nap 1(a gift from Bryan Tsou).

Mutation analysis in *PPP2R1A*

PPP2R1A mutations were quantified from publicly available studies on cBioPortal (Cerami et al., 2012; Gao et al., 2013) as of June 2019.

Cell lysis, immunoprecipitation and phosphatase assays

Frozen cell pellets were suspended in buffer B (30 mM HEPES pH 7.8, 140 mM NaCl, 6 mM $MgCl_2$, 5% glycerol) supplemented with 2 mM DTT, ProBlock Gold Mammalian Protease Inhibitor Cocktail (GoldBio Technology) and PhosSTOP (Roche) and maintained at 4 °C. Samples were lysed by nitrogen cavitation (Parr Instruments) for 5 min at 2,000 psi, and then centrifuged at 20,000 x *g* for 15 min. Proteins were immunoprecipitated with antibody bound to Protein A Dynabeads (ThermoFisher Scientific) for 1 h, washed three times with buffer B, and analyzed by western blot via chemiluminescence using an ImageQuant LAS500 (GE Life Sciences). Image cropping and intensity measurements were performed in Fiji (Schindelin et al., 2012) and images were assembled in Illustrator (Adobe, San Jose, CA). For phosphatase assays, cell pellets were suspended in buffer B with protease inhibitor and DTT. Lysates were mixed with protein G sepharose beads (GE Healthcare) bound to PP2A-Aα IgG or control IgG. After washing in buffer B, samples were split and incubated with 200 nM Okadaic acid or DMSO. A portion was reserved for western blot analysis. The remainder was used in the Ser/Thr phosphatase assay (Promega). Final assay conditions were: 80 μM phosphopeptide, 50 mM imidazole pH 7.2, 0.2mM EGTA, 0.02% β-mercaptoethanol, 0.1

mg/mL BSA ± 144 nM okadaic acid. Phosphatase activity was quantified by absorbance measured at 630 nm on a spectrophotometer.

PP2A-Aα immunoprecipitation for SILAC mass spectrometry analysis

Wild type RPE-1 cells expressing GFP-PP2A-Aα (WT, P179R, or R183W) were grown in DMEM:F-12 (1:1) media for SILAC (ThermoFisher Scientific), supplemented with 10% dialyzed FBS (ThermoFisher Scientific), 1X penicillin-streptomycin (Gemini Bio-Products), 2.5 mM L-Glutamine (Sigma-Aldrich), 0.175 mM Arginine and 0.25 mM Lysine. Arg^0 and Lys^0 amino acids were purchased from Sigma. Arg^{10} ($^{13}C_6/^{15}N_4$ arginine) and Lys^8 ($^{13}C_6/^{15}N_2$ lysine) amino acids were purchased from Cambridge Isotopes. After two weeks of passaging, incorporation of heavy amino acids was measured by mass spectrometry. Samples with 95% or greater incorporation of Lys^8 and Arg^{10} were used in analyses. For immunoprecipitation, asynchronously growing cells were trypsinized, pelleted, and frozen. Cells were thawed and re-suspended in lysis buffer (180 mM NaCl, 50 mM sodium phosphate pH 7.4, 2 mM $MgCl_2$, 0.1% Tween-20, 1X ProBlock Gold Mammalian Protease Inhibitor Cocktail (GoldBio Technology) and 1X Simple Stop 3 phosphatase inhibitor (GoldBio Technology)). All further steps were carried out at 4 °C. Cells were lysed by nitrogen cavitation (Parr Instruments) at 2,000 psi for 10 min, followed by centrifugation at 20,000 x *g* for 20 min. The supernatant was centrifuged once more. 5 mg protein was incubated with 125 µg α-GFP antibody covalently coupled to M270 magnetic resin (ThermoFisher Scientific) for 1 h with rotation. The resin was washed five times with lysis buffer. Bound proteins were eluted into 0.5 N NH_4OH, 0.5 mM EDTA and dehydrated in a vacufuge (Eppendorf).

Dehydrated samples were suspended in 20 µL of NuPAGE LDS sample buffer (ThermoFisher Scientific). SILAC pairs were mixed, denatured at 90 °C for 2 min and separated on a 10% NuPAGE gel (ThermoFisher Scientific) at 120 V for 20 min. The gel was washed and silver stained (Pierce Silver Stain kit). Each lane was excised and destained using 30 mM potassium hexa-cyanoferrate (III) /100 mM sodium thiosulfate, washed and de-hydrated using a vacuum centrifuge. Proteins in the gel slabs were reduced, alkylated with iodoacetamide, dehydrated in a vacuum centrifuge. Gel slabs

were then re-hydrated using 50 mM ammonium bicarbonate pH 8.4 (containing 0.04 µg sequencing grade modified porcine trypsin (Promega)) and incubated for 16 h at 37 ◦C. After proteolysis inhibition and tryptic peptide elution from the polyacrylamide slabs, eluates from each lane were pooled, lyophilized, and stored at −80 ◦C until analysis. The lyophilized peptide pellets were resuspended in 0.1% formic acid/ 3% acetonitrile and 5% of the solution was analyzed by LC/MS. The LC system consisted of a vented trap-elute setup (EasynLC1000, Thermo Fisher scientific) coupled to the Orbitrap Fusion mass spectrometer (Thermo Fisher Scientific, San Jose, CA) via a nano electro-spray DPV-565 PicoView ion source (New Objective). The trap column was fabricated with a 5 cm × 150 µm internal diameter silica capillary with a 2 mm silicate frit, and pressure loaded with Poros R2-C18 10 µm particles (Life Technologies). The analytical column consisted of a 25 cm × 75 µm internal diameter column with an integrated electrospray emitter (New Objective), packed with ReproSil-Pur C18-AQ 1.9 µm particles (Dr. Maisch). Peptides were resolved over 90 min using a 3%–45% gradient acetonitrile/ 0.1% formic acid (buffer B) gradient in a water/0.1% formic acid (buffer A) at 250 nL/minute. Precursor ion scans were recorded from 400–2000 m/z in the Orbitrap (240,000 resolution at m/z 200) with an automatic gain control target set at 10^5 ions and a maximum injection time of 50 ms. We used data-dependent mass spectral acquisition with monoisotopic precursor selection, ion charge selection (2–7), dynamic precursor exclusion (60 s, 20 ppm tolerance) and HCD fragmentation (normalized collision energy 35, isolation window 0.8 Th) using the top speed algorithm with a duty cycle of 2 s. Product ion spectra were recorded in the linear ion trap (“normal” scan rate, automatic gain control = 5000 ions, maximum injection time = 150 ms). Spectra were analyzed using MaxQuant Version1.5.2.8, searching within the human UniProt database (version 01/27-2016) with FDR <0.01. Intensity measurements were normalized to the PP2A-Aα intensity and then SILAC ratios were calculated. Four biological replicates were analyzed. P-values were calculated from a two-tailed student’s *t*-test for proteins identified in three or more experiments. We focused on proteins with $\geq$ 2-fold change in binding and $P < 0.05$. Raw files are openly accessible via PRIDE accession number PXD010709.

SUPPLEMENTAL REFERENCES

Berdougo, E., Terret, M.-E. and Jallepalli, P. V (2009). Functional dissection of mitotic regulators through gene targeting in human somatic cells. *Methods Mol. Biol.* **545**, 21–37.

Cerami, E., Gao, J., Dogrusoz, U., Gross, B. E., Sumer, S. O., Aksoy, B. A., Jacobsen, A., Byrne, C. J., Heuer, M. L., Larsson, E., et al. (2012). The cBio cancer genomics portal: an open platform for exploring multidimensional cancer genomics data. *Cancer Discov.* **2**, 401–4.

Foley, E. A., Maldonado, M. and Kapoor, T. M. (2011). Formation of stable attachments between kinetochores and microtubules depends on the B56-PP2A phosphatase. *Nat Cell Biol* **13**, 1265–71.

Gao, J., Aksoy, B. A., Dogrusoz, U., Dresdner, G., Gross, B., Sumer, S. O., Sun, Y., Jacobsen, A., Sinha, R., Larsson, E., et al. (2013). Integrative analysis of complex cancer genomics and clinical profiles using the cBioPortal. *Sci. Signal.* **6**, pl1.

Nijenhuis, W., Vallardi, G., Teixeira, A., Kops, G. J. P. L. P. L. and Saurin, A. T. (2014). Negative feedback at kinetochores underlies a responsive spindle checkpoint signal. *Nat. Cell Biol.* **16**, 1257–64.

Papi, M., Berdougo, E., Randall, C. L., Ganguly, S. and Jallepalli, P. V (2005). Multiple roles for separase auto-cleavage during the G2/M transition. *Nat. Cell Biol.* **7**, 1029–35.

Schindelin, J., Arganda-Carreras, I., Frise, E., Kaynig, V., Longair, M., Pietzsch, T., Preibisch, S., Rueden, C., Saalfeld, S., Schmid, B., et al. (2012). Fiji: an open-source platform for biological-image analysis. *Nat. Methods* **9**, 676–682.

Wang, W. J., Acehan, D., Kao, C. H., Jane, W. N., Uryu, K. and Tsou, M. F. B. (2015). De novo centriole formation in human cells is error-prone and does not require SAS-6 self-assembly. *Elife* **4**,.